Journal of Applied Polymer Science

# Polyurethanes Containing a Crystalline Polyol and Semiflexible Urethane Segments

**Borja Fernández-d'Arlas,[1] Raquel Fernández,[1] James Runt,[2] Arantxa Eceiza[1]**

[1]Grupo "Materiales+Tecnologías" (GMT), Departamento de Ingeniería Química y del Medio Ambiente, Universidad del País Vasco (UPV/EHU), Pza. Europa 1, 20018 Donostia-San Sebastián, Spain

[2]Department of Materials Science and Engineering, The Pennsylvania State University, University Park, Pennsylvania 16802

Correspondence to: A. Eceiza (E-mail: arantxa.eceiza@ehu.es)

**ABSTRACT:** Ultradrawing semicrystalline polymers is an intriguing approach to develop stiff, strong, and tough polymeric fibers. In the research field of polyurethane copolymer elastomers the term "soft segment" usually refers to the medium molecular weight glycol while the term "hard segment" stands for the urethane rich or isocyanate-short glycol segments. Here we investigate the influence of semiflexible segment content in the urethane rich phase on the mechanical properties and morphology of polyurethanes synthesized with a crystalline polyol as a "soft" segment. Materials with lower semiflexible urethane segment content developed stiffer and stronger materials upon drawing. This was related to greater soft segment crystallization along the draw direction. Materials with a higher fraction of semiflexible urethane segments were more elastic (higher yield strains and strengths) but exhibited more brittle-like fracture. © 2014 Wiley Periodicals, Inc. J. Appl. Polym. Sci. **2015**, *132*, 41281.

**KEYWORDS:** biomimetic; biopolymers and renewable polymers; copolymers; elastomers; polyurethanes

Received 20 May 2014; accepted 7 July 2014

**DOI: 10.1002/app.41281**

## INTRODUCTION

Materials combining strength and elasticity are attractive for a range of applications in which high energy loads can be dissipated before material failure. Examples of these applications include fishing wires, cordage, climbing, paragliding, and parachuting equipment, and tough textiles. In these applications materials exhibiting outstanding stiffness like para(phenyleneamides)[1,2] and ultradrawn polyethylene,[2–4] are widely used. Nevertheless, despite their remarkable stiffness and tensile strength, these materials lack mechanical toughness, or a combination of strength and deformability.

Spider silk is a natural polymer exhibiting remarkable toughness.[5,6] Typical values of strengths and deformability of major ampullate fiber threads are ~1–1.5 GPa[7] and 20–30%, respectively.[8] These values account for the astonishing toughness, usually in the range of 150–250 MJ $m^{-3}$.[6,7] Among synthetic polymers, polyurethanes (PU) can be considered to be one of the toughest materials,[9] usually because of their high elasticity and deformation to break. Contrary to currently used high performance fibers, PUs usually lack appropriate stiffness and strength.[10] Therefore, one of the goals of materials scientists is to create synthetic mimics of spider silk fibers by macromolecular engineering of synthetic polymers such as PUs.[8,11] Like spider silk, PUs are multiblock copolymers consisting on hard and soft segments, and form the primary constituents of the hard and soft phases, respectively. Despite their partial morphological similarity, in most cases the differences in mechanical properties are considerable.[12] Spider silk threads, as other high performance fibers like synthetic polyamides, have a high degree of macromolecular orientation along the fiber axis, as well as high interchain hydrogen bonding.[13] In the case of ultradrawn polyethylene, unlike synthetic or natural polyamides, in addition to high macromolecular orientation, the mechanism governing stiffness and strength is stress transfer achieved by macromolecular entanglements[14] and large number of weak intermolecular bonds. It is conceivable that highly drawn materials incorporating strain-induced crystallinity, along with some degree of hydrogen bonding, would lead to comparable or perhaps even improved mechanical performance as compared to ultradrawn polyethylene or polypropylene. In our previous work we studied different drawn polyurethanes and demonstrated that bulky hard segments, like those containing isophorone diisocyanate (IPDI)[8] or 4,4′-bisphenilene diisocyanate (MDI),[11] are less likely to develop stiff and strong materials after drawing, as compared to those formed by more flexible and crystalline hard segments

Additional Supporting Information may be found in the online version of this article.

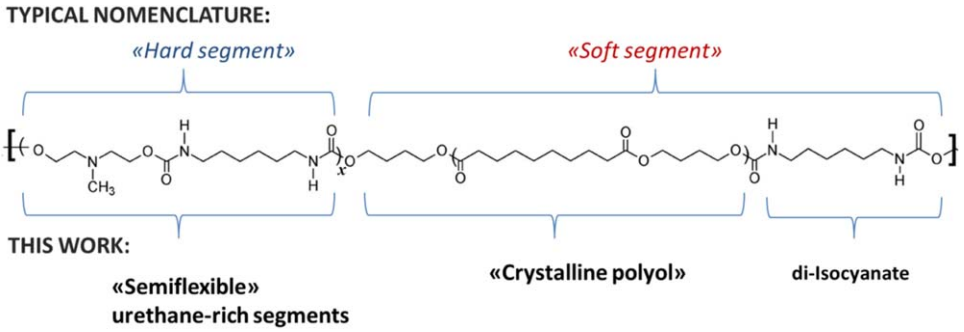


**Figure 1.** General molecular structure of the synthesized PUs. Values of *x* are given in Table I. [Color figure can be viewed in the online issue, which is available at wileyonlinelibrary.com.]

like the ones obtained from 1,6-hexamethylene diisocyanate (HDI) and butanediol (BD) or HDI and *N*-methyl-diethanol amine (MDEA).[15]

In this work, with the aim of unraveling the structure-properties relationships of PU in order to design super-tough materials, we explore the influence of semiflexible hard segment content, formed by HDI–MDEA, on the morphology and mechanical properties of drawn specimens. Materials characterization was carried out using a variety of experimental methods, including Fourier transform infrared spectroscopy (FTIR), tensile mechanical testing, polarized optical microscopy (POM), and wide and small angle X-ray scattering (WAXS and SAXS, respectively).

## EXPERIMENTAL

### Polyurethane Synthesis

The polyurethanes were synthesized in bulk by the common two step polymerization technique under an $N_2$ atmosphere into a three necked glass reactor provided by a mechanical stirrer. The polyol ($T_g = -27°C$, $T_m \sim 65°C$) consisted of a diol synthesized by oligomerization of sebacic acid (derived from castor oil) with ethylene glycol. It is highly crystalline at room temperature and the crystals are spherulitic in nature (Supporting Information Figure S1). The polyol number-average-molecular weight, $M_n$ (1880 g mol$^{-1}$), was determined using a backward titration standard[16] for measuring the hydroxyl number. In the first stage of the polymerization the polyol was reacted at 100°C for 5 h with 1,6-hexamethylene diisocyanate (HDI, Bayer) until a prepolymer was obtained. In the second stage this prepolymer was reacted with the chain extender, N-methyl-diethanol amine (Aldrich), and the mixture was vigorously stirred before being poured into a poly(tetrafluoroethylene) mold to complete polymerization in a press at 100°C for 10 h. By controlling the stoichiometry between the reactants, materials with different proportions of urethane rich semiflexible segments were obtained. Figure 1 represents the general structure of the synthesized PUs, with different degree of hard segment polymerization, *x*. Table I gathers reactant molar ratios as well as some molecular weights and soft phase glass transition temperatures of the PUs. The samples are named as "PU" plus the weight fraction of semiflexible urethane segments. For example PU64 contained 64 wt % of (HDI-MDEA) units to respect of the total weight the repetitive structure.

### Size Exclusion Chromatography

The molecular weights and molecular weight distributions were analyzed by size exclusion chromatography (SEC) using a Perkin Elmer chromatograph equipped with a binary pump and a refractive index detector. THF was used as the mobile phase and the separation was carried out within four columns packed with particle gels with different nominal pore sizes. Elution rate was 1 mL min$^{-1}$ and experiments were performed at room temperature. The samples were dissolved to ~1 wt % in tetrahydrofuran (THF). The molecular weights and molecular weight distributions were based on a calibration curve with monodisperse polystyrene standards.

### Infrared Spectroscopy

The PUs structure was analyzed by Attenuated total reflectance Fourier transformed infrared spectroscopy (ATR–FTIR) using a Golden Gate accessory device mounted in a Nicolet-Nexus-FTIR spectrometer. Spectra were obtained between 4000 and 400 cm$^{-1}$ by averaging 20 scans with a resolution of 2 cm$^{-1}$.

### Material Drawing and Tensile Testing

Samples for tensile testing were die cut from hot pressed films, prepared by heating up to 180°C for 5 min with pressure, followed by slow cooling to 30°C. Specimens of ~2.5 × 0.1 mm$^2$ cross-sections were drawn onto the mechanical testing machine (MTS-Insight10) to different drawn ratios, $\lambda$. The draw ratios

**Table I.** PUs Composition, Molecular Weight, and Soft Phase Glass Transition Temperature

| PU | HDI/MDEA/Polyol | *x* | $M_w$ (g mol$^{-1}$) | $M_w/M_n$ | $M_{w,max}$ (g mol$^{-1}$) | $T_{g,\ SS}$ |
|---|---|---|---|---|---|---|
| PU12 | 4/1/3 | 1/3 | 68,600 | 2.0 | 480,000 | −44 |
| PU19 | 2/1/1 | 1 | 48,500 | 1.9 | 238,000 | −42 |
| PU30 | 3/2/1 | 2 | 31,500 | 1.1 | 130,600 | −38 |
| PU41 | 5/4/1 | 4 | 27,200 | 1.2 | 95,100 | −25 |
| PU64 | 9/8/1 | 8 | ~15,000 | 1.1 | 123,800 | −17 |

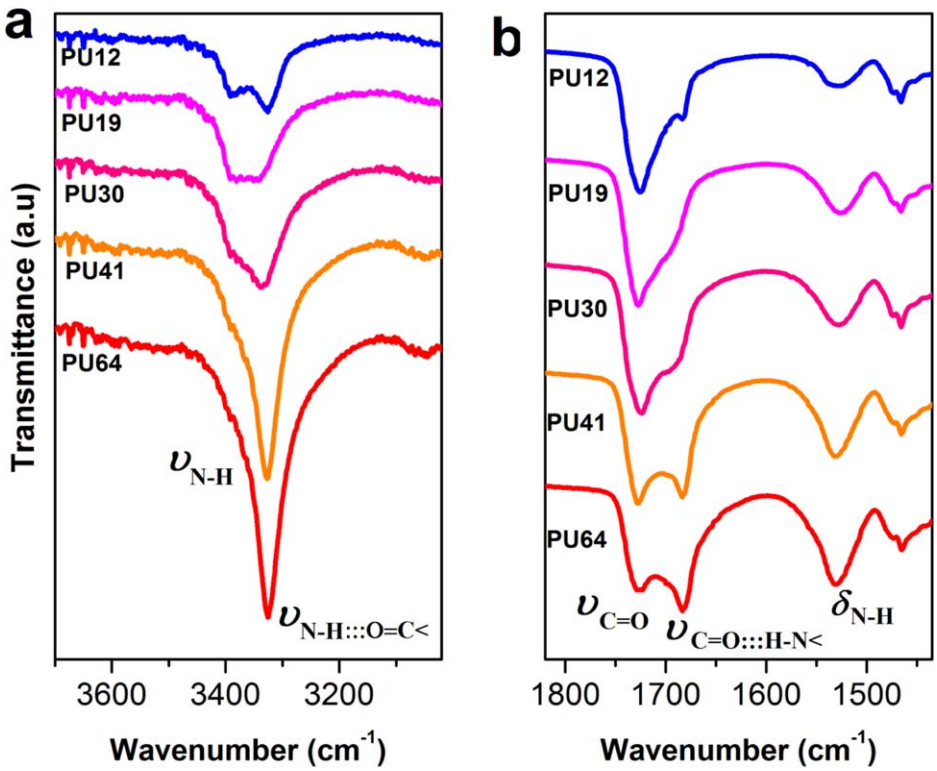


**Figure 2.** ATR–FTIR spectra of the synthesized PUs. (a) Amide (N—H) stretching region and (b) carbonyl (C═O) stretching region. [Color figure can be viewed in the online issue, which is available at wileyonlinelibrary.com.]

explored were $\lambda = 4$ and 7. Tensile tests of both pristine and drawn samples were carried out at a crosshead speed of 100 mm $min^{-1}$ using a MTS-Insight 10 instrument equipped with pneumatic grips (Advantage pneumatic grips) with an initial cross-head gap of ~8 mm and with a 250 N load cell. The thicknesses and widths of the drawn samples were measured again after drawing and then clamped in such a way that only the drawn material experienced the tensile stress. At least three specimens were tested for each sample. Yield points were determined from the strain–stress curves by taking the yield strain as the point close to the intercept of the tangent in the elastic regime with that in the pseudo-plastic regime. In the cases were there was a clear drop in stress after yielding, the yield point was taken at the point in which $d\sigma/d\varepsilon = 0$.[17]

### Differential Scanning Calorimetry

Differential scanning calorimetry (DSC) was performed between −60 and 250°C on a Mettler Toledo calorimeter at a heating rate of 20°C $min^{-1}$ under constant $N_2$ flow. Samples were analyzed before and after being drawn to $\lambda = 3$, 5, and 7 and then relaxed at those strains for 10 min. Specimens of ~1–4 mg were cut, weighed, and placed in aluminum DSC pans.

### Polarized Optical Microscopy

For optical structural analysis samples were deformed and held in a small home designed stretching device (Suguz, Donostia-San Sebastián, Spain) consisting of two clamps and a screw guide with submillimeter precision to control strain. Samples cast from 50 mg $mL^{-1}$ THF solutions were inserted between crossed-polarizers and observed.

### X-ray Scattering

To analyze the structure evolution with strain from the molecular level to the supramolecular scale, two scattering experiments were conducted. WAXS provided information on polyurethane segment arrangements with respect to the others while SAXS was used to explore supramolecular level nanodomain arrangements. WAXS patterns were measured on a Rigaku DMAX/Rapid microdiffractometer in transmission mode, using a copper point-focused source ($\lambda$= 0.154 nm) at 50 kV and 40 mA. For analysing materials at specified elongations, an extension rig was used as explained elsewhere.[18,19] WAXS diffraction angles were converted to wavevector ($q$) by using $q = 4\pi\sin\theta/\lambda$. SAXS data were collected with a Molecular Metrology instrument with a CuK$\alpha$ radiation source ($\lambda = 0.154$ nm) at 45 kV and 65 mA, using a two dimensional multiwire detector with a sample-to-detector distance of 1.5 m. The average interdomain long spacing, was calculated from SAXS data using the Bragg formula, $d = 2\pi/q_{max}$, where $q_{max}$ is the scattering vector of the maximum in the Lorentz-corrected intensity, $q^2I(q)$. The equator of the WAXS and SAXS scattering patterns was defined as the direction perpendicular to strain and lays in the horizontal direction on the 2D patterns to be shown later, and at which the azimuthal angle was taken as $\psi = 0$. The meridian is the direction parallel to the draw direction.

### Laser Transparency

Films for laser transparency measurements were placed on the home made stretching device and set between two polarizers. The laser (632.8 nm, He—Ne) intensity through the films sandwiched between parallel and crossed-polarizers was analyzed.

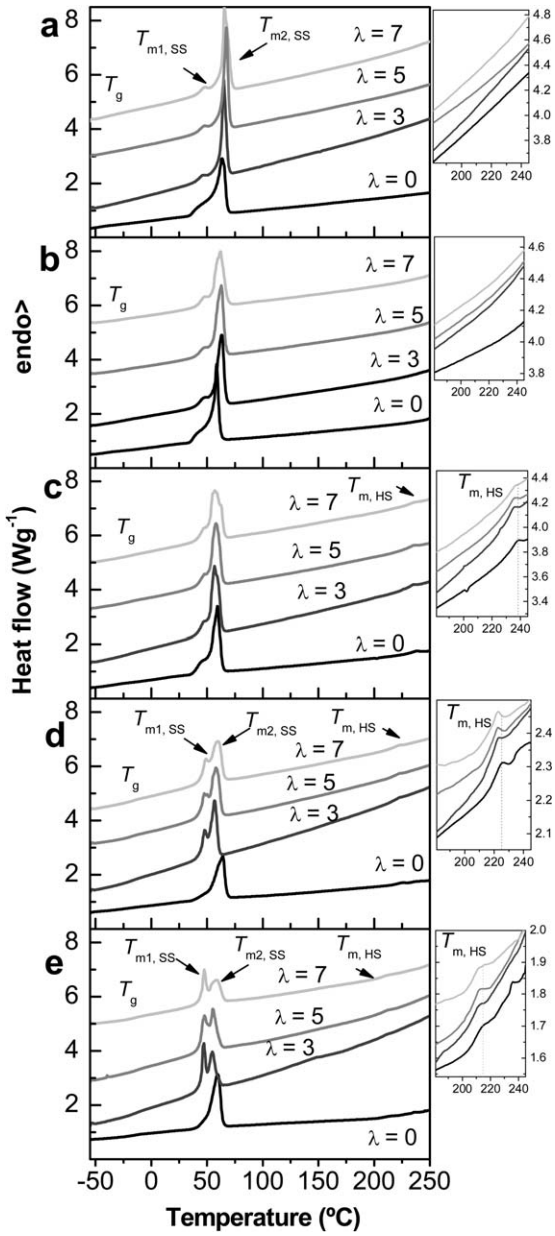


**Figure 3.** DSC heating scans of materials drawn to the indicated ratios. (a) PU12, (b) PU19, (c) PU30, (d) PU41, and (e) PU64. Zooms to the right correspond to the high temperature range.

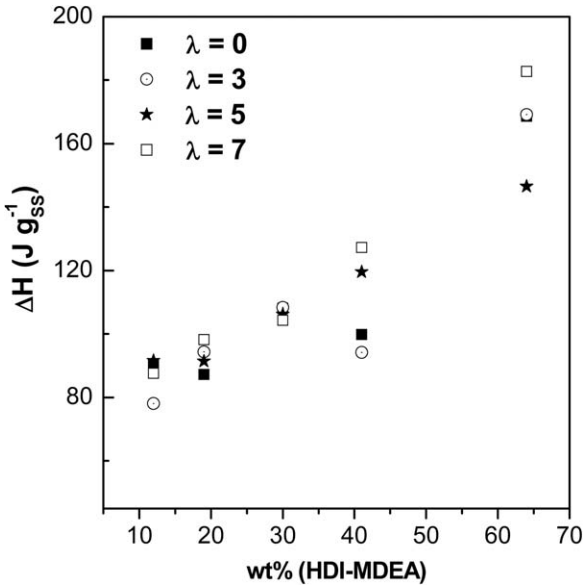


**Figure 4.** Soft phase melting enthalpy normalized to respect the soft segments weight fraction (polyol weight fraction) represented against the (HDI–MDEA) fraction in the PU. Values at different values of stretching, $\lambda$.

The light intensity passing through the samples at different strains was normalized with respect to the intensity passing through the non-strained samples. In this way, the intensity with parallel polarizers, $<|I_p|>$, was defined as $<|I_p|> = (I_{p,L}/d_L)/(I_{p,L0}/d_{L0})$ and the intensity with crossed polarizers was defined as $<|I_c|> = (I_{c,L}/d_L)/(I_{c,L0}/d_{L0})$, where $I_{p,L}$ and $I_{c,L}$, are intensities passing through the samples at different strain with parallel and crossed polarizers, respectively, and $I_{p,L0}$, $I_{c,L0}$ are the intensities passing through the nonstrained samples with parallel and crossed-polarizer, respectively. $d_L$ and $d_{L0}$ are the thickness of strained and nonstrained samples, respectively. The laser set-up scheme is depicted in Figure 8(a) of the Results and Discussion section. Intensities were measured for three different specimens and averaged.

## RESULTS AND DISCUSSION

### Structural Characterization

The synthesized PUs were analyzed by FTIR in order to check for any traces of unreacted isocyanate groups. No isocyanate absorption peak at ~2270 cm$^{-1}$ was found for any of the

**Table II.** Variation of Melting Endotherm Enthalpy with Composition and Strain

| Polyurethane | | $\lambda = 0$ | | $\lambda = 3$ | | $\lambda = 7$ | |
|---|---|---|---|---|---|---|---|
| PU | wt % Polyol | $\Delta H_{\lambda=0}$ (J $g^{-1}_{PU}$) | $\Delta H_{\lambda=0}$ (J $g^{-1}_{Polyol}$) | $\Delta H_{\lambda=3}$ (J $g^{-1}_{PU}$) | $\Delta H_{\lambda=3}$ (J $g^{-1}_{Polyol}$) | $\Delta H_{\lambda=7}$ (J $g^{-1}_{PU}$) | $\Delta H_{\lambda=7}$ (J $g^{-1}_{Polyol}$) |
| PU12 | 88 | 79.3 | 90.1 | 68.7 | 78.1 | 80.6 | 91.6 |
| PU19 | 81 | 70.7 | 87.2 | 76.4 | 94.3 | 74.0 | 91.4 |
| PU30 | 70 | 75.7 | 108.1 | 75.9 | 108.4 | 74.3 | 106.1 |
| PU41 | 59 | 58.9 | 99.8 | 55.6 | 94.2 | 70.5 | 119.5 |
| PU64 | 36 | 60.7 | 168.5 | 60.9 | 169.1 | 52.7 | 146.5 |

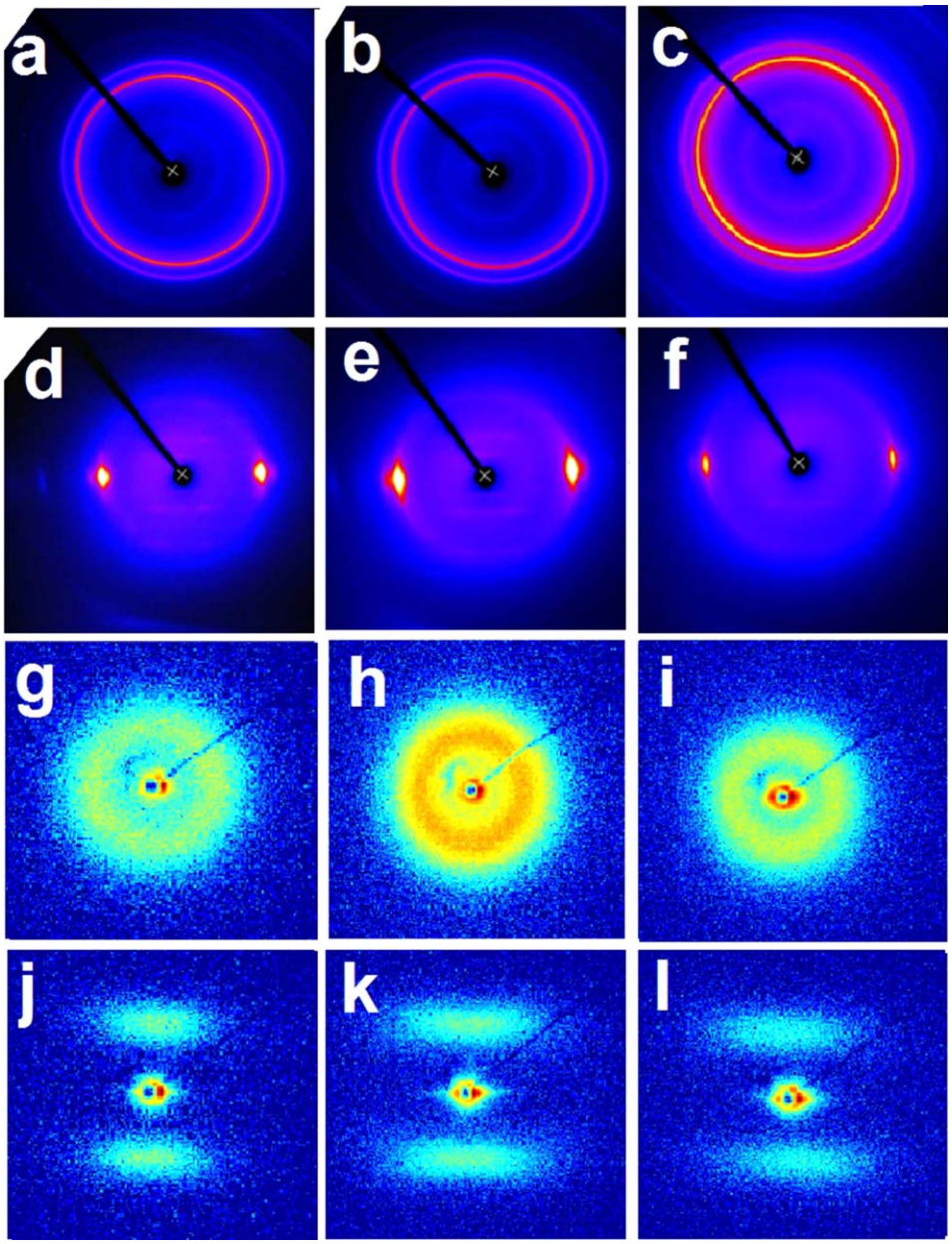


**Figure 5.** WAXS diffraction patterns of nondeformed (a) PU12, (b) PU19, and (c) PU30; and of (d) PU12, (e) PU19, and (f) PU30 at $\lambda = 5$. (g–i) SAXS patterns of nondeformed PU12, PU19, and PU30, respectively. (j–l) SAXS patterns of deformed PU12, PU19, and PU30 at $\lambda = 5$, respectively. Tensile deformation is vertical. [Color figure can be viewed in the online issue, which is available at wileyonlinelibrary.com.]

materials suggesting complete polymerization.[20] FTIR was also useful for characterizing local PU structure, providing information on the state of hydrogen bonding. As seen in Figure 2(a), the spectra in the amide N—H stretching region varied as a function of PU stoichiometry. The lower frequency band at 3327 $cm^{-1}$ increased systematically in intensity as the fraction of urethane rich segments increased, indicative of more ordered hydrogen bonded N—H species with increasing urethane rich segments.[21–23] Likewise, the higher frequency band at ~3400 $cm^{-1}$, associated with disordered N—H hydrogen bonds, decreases in relative intensity. The carbonyl stretching region of the spectra [Figure 2(b)] is somewhat more complicated to interpret due to a contribution from the C═O in the ester functionality in soft segments at ~1720–1710 $cm^{-1}$, but nevertheless a relative systematic increase in absorbance of order hydrogen bonded urethane C═O was observed at 1680 $cm^{-1}$ with increasing content of urethane rich segments. Clearly, from both the N—H and C═O regions of the spectra, the degree of local molecular order increases with increasing fraction of urethane containing hard segments. In the region 1550–1450 $cm^{-1}$ and increase of the intensity of N—H bending was observed with the increase of urethane rich segment as a consequence of the compositional enrichment of this functional group into the PU.

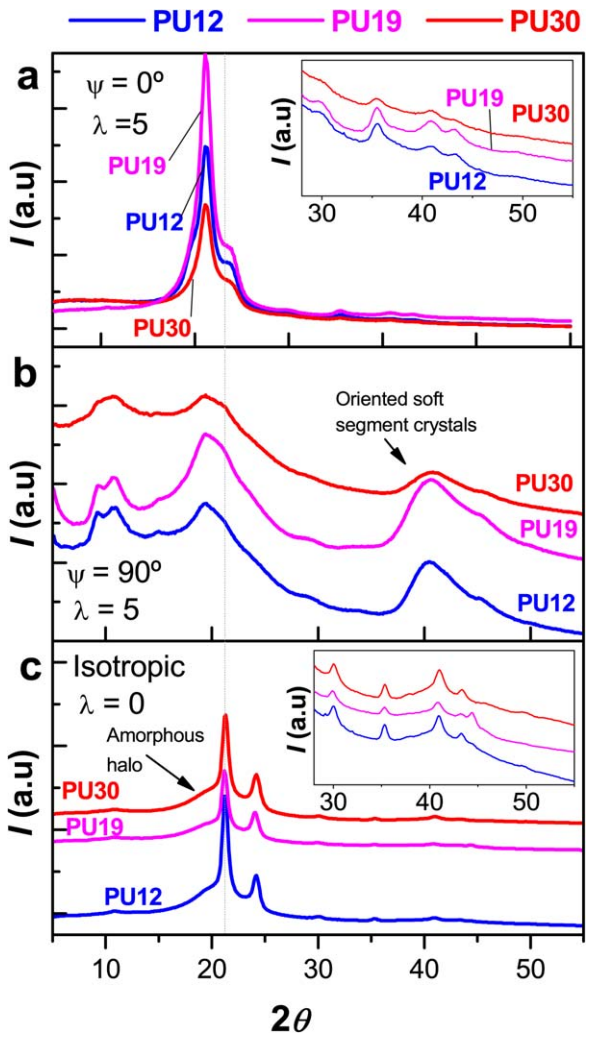


**Figure 6.** WAXS intensity profiles of PU12, PU19, and PU30 as integrated (a) equatorially for samples at $\lambda = 5$, (b) at the meridian at $\lambda = 5$, and (c) isotropically for the undeformed sample. [Color figure can be viewed in the online issue, which is available at wileyonlinelibrary.com.]

The melting of soft segment crystals is evident in the differential scanning calorimetry thermograms near 50–60°C (Figure 3). As can be observed in data gathered in Table II, materials with higher semiflexible urethane rich segments exhibited lower overall soft segment crystallinity (79 J $g^{-1}$ melting enthalpy for PU12 versus 61 J $g^{-1}$ for PU64). However, when normalizing this endotherm enthalpy to the soft segment weight fraction into the polymer (considered as the pure polyol weight fraction), PUs with higher HDI-MDEA contents exhibit a significantly higher melting enthalpy per gram of soft segment. This is displayed in Figure 4, where the soft segment weight fraction normalized enthalpy is represented against the weight fraction of (HDI–MDEA) units into the PU. This is a surprising finding. One might initially propose that at higher hard content there is greater unlike segment segregation, with the soft phase becoming enriched in polyol and can more readily crystallize. However, as discussed below, the soft phase $T_g$ increases with increasing hard segment content, suggesting greater hard/soft mixing at higher hard segment content. The origin of the relative increase in soft segment crystallinity remains unclear but we speculate that this may arise from HDI–MDEA segments participating in the formation of more cohesion structures, for example through the formation of hydrogen bonds with soft segments.

In Figure 4, it can also be seen that uniaxial stretching did not induce appreciable changes in soft segment crystallization. This may be due to the moderate drawing ratios used in this work, since previously we demonstrated that drawing PU30 up to $\lambda = 16$ led to strain induced crystallization.[8] Nevertheless, as can be observed in Figure 3, the soft segment crystal melting transition varied notably after drawing, suggesting strain-induced morphological transformations. Materials with 64 and 41 wt % hard segments display multiple melting endotherms after drawing, with melting temperatures in the region between 40 and 70°C, labeled as $T_{m1,SS}$ and $T_{m2,SS}$. These likely arise from two populations of crystals with different mean crystal thicknesses. Upon stretching PUs rich in semiflexible urethane segments [Figure 3(d–e)], the endotherm $T_{m1,SS}$ increases in relative intensity, suggesting formation of soft segment crystalline regions with "defective" structures or thinner lamella. In addition, as can be seen in the higher temperature insets to the right of Figure 3, morphological changes involving crystallization of semiflexible hard segments, HDI–MDEA, are likely to occur in materials with a high fraction of these segments. The endotherm, labeled as $T_{m,HS}$, appearing between 215 and 240°C, is related to urethane rich segments, since this endotherm appears only in PUs with high HDI-MDEA contents. The temperature range of this endotherm decreased as HDI-MDEA content increased.

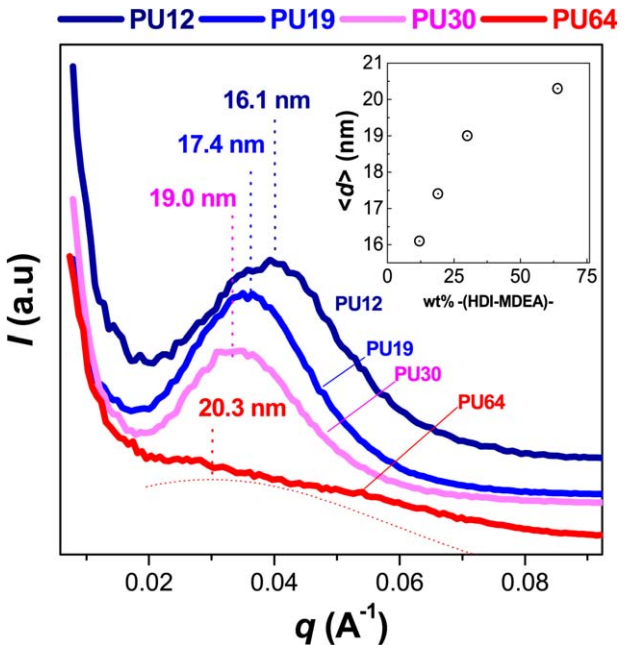


**Figure 7.** SAXS scattering profiles of nondeformed PU12, PU19, PU30, and PU64, indicating the interdomain spacing for each case. The red dotted curve is a Gaussian fit to PU64 curve. Inset shows interdomain spacing as function of HDI–MDEA weight fraction into the PU. [Color figure can be viewed in the online issue, which is available at wileyonlinelibrary.com.]

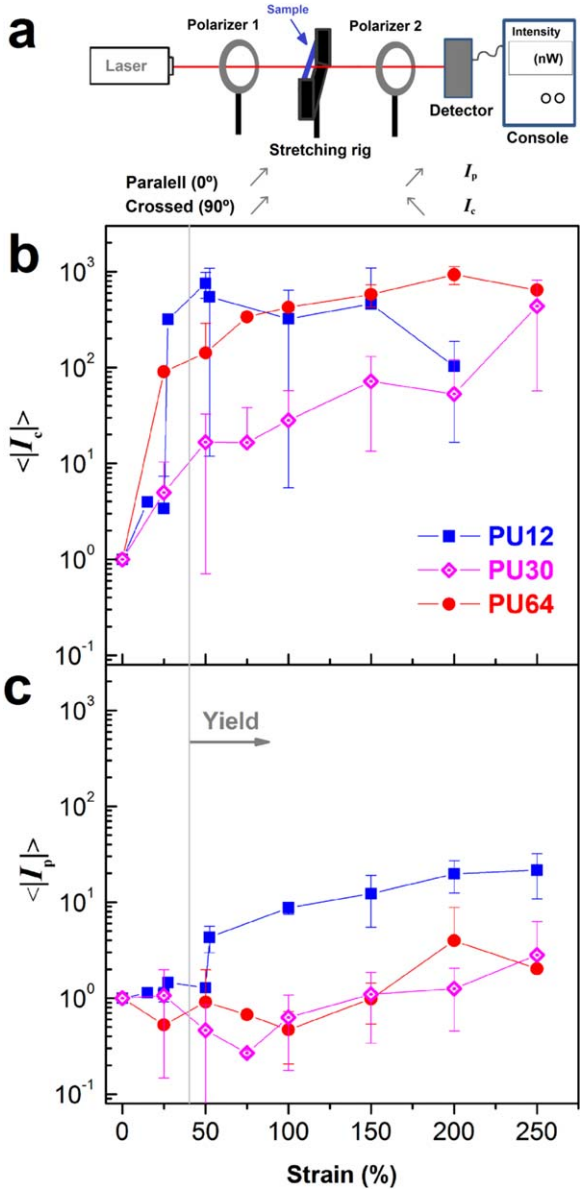


**Figure 8.** Laser transparency analysis. (a) Set-up scheme. Variation of laser transparency for PU12, PU30, and PU65 with strain with (b) crossed polarizers and (c) parallel polarizers. [Color figure can be viewed in the online issue, which is available at wileyonlinelibrary.com.]

A significant increase in the soft phase glass transition temperature, $T_{g,SS}$, was noted with increasing urethane hard segment content: from −44°C for PU12 to −17°C for PU62 (Table I). This is likely related at least partially to the enrichment of semi-flexible hard segments in the soft phase ($T_g \sim -10$°C for the pure HDI–MDEA polymer). Upon stretching, these transition shift to slightly higher temperatures (i.e., from −44 to −39°C for PU12 from −17 to −14°C for PU62 stretched to $\lambda = 7$). This increase is consistent with a small amount of strain induced phase mixing and constrain of the soft segments.[17]

Two dimensional WAXS patterns of three selected PUs in the undeformed and deformed ($\lambda = 5$) states are shown in Figure 5(a–f). Undeformed samples showed concentric isotropic scattering rings, while stretched specimens displayed sharp equatorial arcing ($\psi = 0°$, $2\theta = 21°$), indicative of the overall orientation of hard and soft segments in the draw direction. Although somewhat difficult to see in the color images in Figure 6, scattering along the meridional ($\psi = 90°$) and at higher $2\theta$ (~40°) were intensified after stretching suggesting orientation of crystalline soft segments. Integrated 1D patterns at different azimuthal angles are shown in Figure 6. As can be seen in the diffraction pattern of the undeformed PU12, PU19, and PU30 in Figure 6(c), there are two strong diffraction peaks arising from soft segment crystallinity at $2\theta \sim 21°$ and 24°, superimposed on a relatively broad amorphous halo. The peak positions of the crystalline reflections are virtually the same for all compositions, indicating that the soft segment crystal unit cell is nearly identical for each of these materials. As can be appreciated both in Figure 5(a–c) and in Figure 6(c), the contribution of the amorphous halo to the scattering increases somewhat as HDI–MDEA weight fraction increases. This is expected since the soft segment crystals constitute a smaller portion of the system at higher hard segment contents. Note that the peak at $2\theta = 24°$ is only seen as a small shoulder after drawing, likely indicative of less ordered crystalline soft segments after stretching. Disruption of crystalline structures upon stretching is also observed in the region $2\theta = 30°$–50° as can be appreciated by comparing insets in Figure 6(a,c).

SAXS, sensitive to the phase separated structure at the nanoscale, revealed dramatic morphological changes at this length scale. As seen in Figure 5(g–i), nondeformed samples exhibit isotropic scattering rings and 1D scattering profiles are shown in Figure 7. For PU12, PU19, and PU30 these rings correspond to average interdomain distances, $<d>$, of 16.1, 17.4, and 19.0 nm, respectively. The increase in interdomain spacing with the MDEA content suggests that the principal SAXS scattering is produced by soft crystals that become more separated with increased HDI–MDEA content. After stretching materials to $\lambda = 5$, the scattering was concentrated along the meridian ($\psi = 90°$), parallel to the deformation direction. Similar SAXS and WAXS behavior has been observed previously for other polyurethane[11,24] and poly(urea-urethane)[17,25] systems and is attributed to domain orientation and orientation of chains along the deformation direction.[4,26] Nondeformed samples present isotropic distribution of crystalline lamella while progressive increase in strain promotes orientation of chains parallel to strain and lamella orientation and breakdown.[4] The fact that SAXS of deformed samples appears more intense at meridional angles suggests that the scattering patterns of stretched specimens are governed by the disruption and orientation of soft segment lamellas, that form domains that also contribute to electron density variances.

To quantify the observed strain induced transparency of the materials and to relate it to chemical composition, samples were placed between two polarizers and the transmitted intensity of a laser beam through them was analyzed at different strains. Normalized intensities at different strains with polarizers set perpendicular and parallel to each other are shown in Figure 8(b,c), respectively. In all cases it is observed that after yielding (~25–35% deformation) material transparency increased notably. With crossed polarizers this increment was of about two

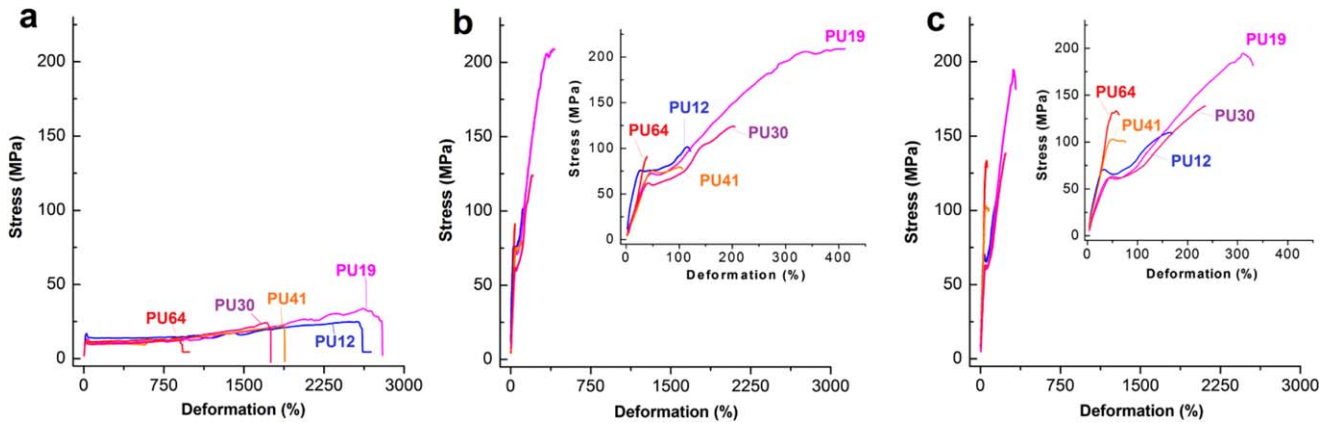


**Figure 9.** Representative stress–strain curves for all PUs. (a) Nonprestretched samples, (b) drawn to $\lambda = 4$ and (c) drawn to $\lambda = 7$. [Color figure can be viewed in the online issue, which is available at wileyonlinelibrary.com.]

orders of magnitude. It was also seen that $<|I_c|>$ increased more with strain for PU12 and PU64 than for PU30. This result may be related to the observations made by crosspolarized optical microscopy (Supporting Information Figure S2), where brighter reflections were seen in samples with extreme compositions (i.e., PU12 and PU64). With parallel polarizers, the intensity, $<|I_p|>$, provides an idea of materials transparency. As observed in Figure 8(c), PU12 exhibited much higher strain induced transparency than PU30 and PU65. This fact was also seen macroscopically with the naked eye. The strain induced transparency in PU12 and the other PUs is likely due to crystal or domain disruption, leading to smaller features that do not scatter light.

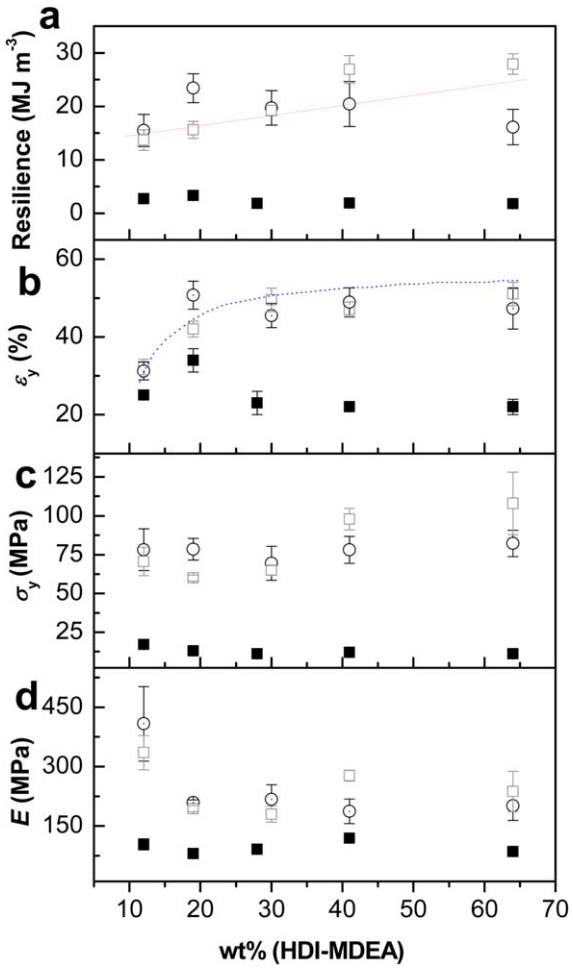


**Figure 10.** Summary of low deformation mechanical properties of PUs as function of HDI–MDEA content. (a) Resilience, (b) yield strain, (c) yield stress, and (d) elastic modulus. (■) Nondrawn samples, (○) drawn to $\lambda = 2$, (□) drawn to $\lambda = 7$. [Color figure can be viewed in the online issue, which is available at wileyonlinelibrary.com.]

### Mechanical Properties

Representative stress–strain curves of selected PUs prior to drawing are shown in Figure 9(a). In Figure 9(b,c) representative curves of the same materials previously drawn to $\lambda = 4$ and $\lambda = 7$ are displayed. Comparing Figure 9(a–c), the dramatic effect of the drawing treatment is readily seen. Note particularly the outstanding combination of strength and deformability of PU19 after predrawing. Although the reason for this is not clear, it is believed to be a consequence of the combination of adequate PU19 molecular weight and hard segment polymerization degree. In general, materials with lower HDI–MDEA wt % exhibit greater plasticity while those with higher wt % of HDI–MDEA display lower strains to break. Statistical values of material tensile properties are gathered in Figures 10 and 11.

As can be seen in Figure 10, the low strain mechanical response to tensile deformation of nondrawn PUs was very similar for all materials. Conversely, after drawing treatments at $\lambda = 4$ and $\lambda = 7$, mechanical response was highly dependent on HDI–MDEA content. The stiffness of the PU12 was greatly increased with prestretching, with an elastic modulus of ~400 MPa. This can be related to the strain induced morphological changes, with molecular chains and soft segment lamella oriented parallel and perpendicular to stress direction, respectively, as noted previously in the morphology analysis section. It is interesting to highlight that this strengthening is solely attributed to morphological changes and not to strain induced crystallization since in the applied predrawing regime this phenomena does not exist as observed by DSC. The yield stress of drawn materials was not markedly influenced by HDI–MDEA wt % for compositions

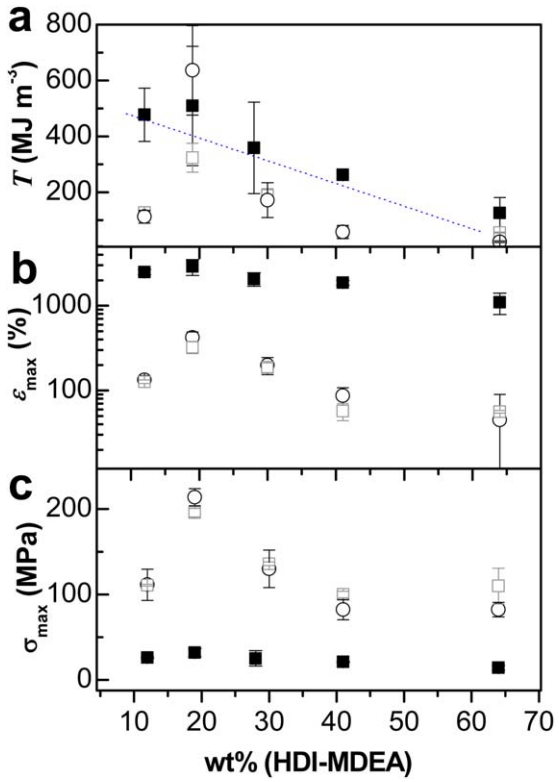


**Figure 11.** Summary of PUs properties at break as function of HDI–MDEA content. (a) Toughness, (b) extensibility, and (c) tensile strength. (■) Nondrawn samples, (○) drawn to $\lambda = 2$, (□) drawn to $\lambda = 7$. [Color figure can be viewed in the online issue, which is available at wileyonlinelibrary.com.]

above 41 wt % HDI-MDEA, where a notably increase was observed upon stretching [Figure 9(c)]. This can be a result of the incorporation of more units capable of hydrogen bonding and therefore to a higher cohesive energy of the materials with higher HDI–MDEA fractions. Interestingly, yield strain also increased with HDI–MDEA wt %. In other PU systems the increase in yield stress achieved when increasing hard segment content is usually accompanied by a decrease in yield strain.[27] This particular behavior can be related to the semiflexible nature of the HDI–MDEA segments, which in addition to hydrogen bonding they also contribute to the rubbery behavior of the PUs. This phenomenon may therefore be exploited to develop new highly resilient materials. As seen in Figure 10(a), the resilience of the PUs was highly increased by prestretching and was higher in PU with higher HDI-MDEA units.

Materials tensile properties at break were more dependent on PUs composition, as can be appreciated in Figure 11. Specially, as seen in Figure 11(b), the extensibility to fracture was substantially affected by PUs composition, therefore affecting materials toughness, $T$ [Figure11(a)]. This phenomenon can be connected with PUs molecular weight, which decreases as higher fractions of HDI–MDEA segments are incorporated. Decrease in PU molecular weight with increased urethane rich fraction is a well-known tendency in PU synthesis. Materials tensile strength was markedly improved with prestretching treatments, as can be observed in Figure 11(c). Variation of prestretching ratio from $\lambda = 2$ to $\lambda = 7$ did not seem to further increase strength. PU19 displayed a markedly high strength of ~200 MPa when drawn. In comparison to the rest of materials, this high strength could be related to a combination of high molecular weight and appropriate hydrogen bonding between HDI–MDEA sequences.

In view of mechanical properties developed after prestretching treatment of PUs with high HDI–MDEA fractions, despite their relatively lower molecular weight, it is envisioned that macromolecules of such nature but with higher molecular weight should develop mechanical properties that could rival those of other known synthetic polymeric fibers.

## CONCLUSIONS

Materials with a crystalline polyol and different amounts of semiflexible urethane rich segments were synthesized and characterized by different experimental techniques. Introduction of semiflexible urethane rich segments increased hydrogen bonding at the same time as yield strain and yield strength, and therefore resilience. Although a decrease in relative molecular weight with incorporation of HDI–MDEA segments negatively affects the toughness, it is believed that high molecular weight materials incorporating semiflexible urethane rich segments in combination with other crystalline segments would develop excellent mechanical properties.

## ACKNOWLEDGMENTS

B. Fernández-d'Arlas acknowledges the University of the Basque Country, (UPV/EHU) post-doc grant "*Ayuda a la Especialización de Doctores*" for its financial support and all authors acknowledge the General Research Services of the University of the Basque Country (SGIker), and especially *Macroconducta-Mesoestructura-Nanotecnología* unit for their technical support. Authors also acknowledge funding from Basque Government in the frame of *Grupos Consolidados* (IT-776-13). B. Fernández-d'Arlas also acknowledges a UPV/EHU post-doctoral mobility grant for accomplishing a 3 months stay at Penn State University. Authors are very thankful to Dr. Raegan Johnson, Dr. Nichole Wonderling and Dr. Autchara Pangon for their help with X-ray instrumentation and techniques. JR would like to thank the National Science Foundation, Polymers Program for support of the portion of this research conducted at Penn State, under grant DMR-1206571.

## REFERENCES

1. García, J. M.; García F. C.; Serna, F.; de la Peña J. L. *Prog. Polym. Sci.* **2010**, *35*, 623.
2. Beers, D.; Young, R. J.; So, C. L.; Sikkema, D. J.; Perepelkin, K. E.; Weedon, G. In High-Performance Fibres; Hearle, J. W. S., Ed.; CRC Press: Boca Raton, **2001**, pp 93–155.
3. Butler, M. F.; Donald, A. M.; Bras, W.; Mant, G. R.; Derbyshire, G. E.; Ryan, A. *J. Macromolecules* **1995**, *28*, 6383.
4. Romo-Uribe, A.; Manzur, A.; Olayo, R. *J. Mater. Res.* **2012**, *27*, 1351.
5. Denny, M. *J. Exp. Biol.* **1976**, *65*, 483.

6. Elices, M.; Plaza, G. R.; Pérez-Rigueiro, J.; Guinea, G. V. *J. Mech. Behav. Biomed. Mater.* **2011**, *4*, 658.
7. Pérez-Rigueiro, J.; Elices, M.; Antón, J.; Guinea, G. V. *Anal. Mecan. Fract.* **2003**, *20*, 421.
8. Blackledge, T. A.; Hayashi, C. Y. *J. Exp. Biol.* **2006**, *209*, 2452.
9. Fernández-d'Arlas, B.; Ramos, J. A.; Saralegi, A.; Corcuera, M.; Mondragon, I.; Eceiza, A. *Macromolecules* **2012**, *45*, 3436.
10. Mishra, A.; Aswal, V. K.; Maiti, P. *J. Phys. Chem. B.* **2010**, *114*, 5292.
11. Fontaine, L.; Ménard, L.; Brosse, J.-C.; Sennyey, G.; Senet, J. P. *React. Funct. Polym.* **2001**, *47*, 11.
12. Fernández-d'Arlas, B.; Corcuera, M.; Runt, J.; Eceiza, A. *Polym. Int.* **2013**, *63*, 1278.
13. Plaza, G. R.; Pérez-Rigueiro, J.; Riekel, C.; Perea, B.G.; Angulló-Rueda, F.; Burghammer, M.; Guinea, G. V.; Elices, M. *Soft Matter.* **2012**, *8*, 6015.
14. Peterlin, A. In The Strength and Stiffness of Polymers; Zachariades, A. E.; Porter, R. S., Eds.; New York and Basel: Marcel Dekker, **1983**; pp 97–128.
15. Fernández-d'Arlas, B.; González, I.; Eceiza, A. *Rev. LatinAm. Metal. Mat.* **2015**, *35*.
16. ASTM-D 4274-88. Standard Test Methods for Testing Polyurethane Raw Materials: Determination of Hydroxyl Numbers of Polyols.
17. Ward, I. M.; Sweeney, J. In An Introduction to the Mechanical Properties of Solid Polymers, 2nd ed.; Wiley: Chichester, England, **2004**; pp 249–250.
18. Lee, H. K.; Fragiadakis, D.; Martin, A. M.; Milne, J.; Runt, J. *Macromolecules* **2010**, *43*, 3125.
19. Choi, T.; Fragiadakis, D.; Roland, C. M.; Runt J. *Macromolecules* **2012**, *45*, 3581.
20. Fernandez d'Arlas, B.; Rueda, L.; Stefani, P. M.; de la Caba, K.; Mondragon, I.; Eceiza, A. *Thermochimica Acta* **2007**, *459*, 94.
21. Sung, C.; Schneider, N. *Macromolecules* **1975**, *8*, 68.
22. Cesteros, L. C. *Rev. Iberoamerc. Polím.* **2004**, *5*, 111.
23. Yilgör, E.; Yilgör, I.; Yurtsever, E. *Polymer* **2002**, *43*, 6551.
24. Kojio, K.; Matsuo, K.; Motokucho, S.; Yoshinaga, K.; Shimodaira, Y.; Kimura, K. *Polym. J.* **2011**, *43*, 692.
25. Yeh, F.; Hsiao, B. S.; Sauer, B. B.; Michel, S.; Siesler, H. W. *Macromolecules* **2003**, *36*, 1940.
26. Butler, M. F.; Donald, G. E.; Ryan, A. *J. Polymer* **1995**, *38*, 5521.
27. Rueda-Larraz, L.; Fernández-d'Arlas, B.; Tercjak, A.; Ribes, A.; Mondragon, I.; Eceiza, A. *Eur. Polym. J.* **2009**, *45*, 2096.